JOURNAL OF MATERIALS SCIENCE 24 (1989) 1594–1598

Extended defects in sintered AlN

M. F. DENANOT, J. RABIER
Laboratoire de Métallurgie Physique U.A.131 CNRS, Faculté des Sciences, 86022 Poitiers Cédex, France

Extended defects in the AlN grains of sintered material have been studied by transmission electron microscopy (TEM) as a function of the concentration of sintering additives (Y_2O_3). Evidence of dislocations and planar defects has been found. Using the weak beam technique, dislocations were found to be dissociated in the basal plane. The deduced reduced stacking fault energy, γ', has been found to confirm the correlation between γ' and the charge redistribution index in III-V and II–VI compounds. The formation of planar defects during sintering is also discussed.

1. Introduction

AlN is a semiconductor material with a large band gap (6.02 eV) which crystallizes in the würtzite structure ($a = 0.3111$ nm and $c/a = 1.6$). It is used as a highly refractory ceramic ($T_M = 2773$ K). It exhibits excellent thermal conductivity, good electrical insulation characteristics and a coefficient of thermal expansion closely matching that of silicon in the temperature range 20 to 200° C [1, 2]. This explains why AlN is a prime candidate for VLSI device substrates. However, the high thermal conductivity, measured on single crystals, has not been achieved yet in practice on sintered materials which have to be used as substrates. Defects present in the sintered material are thought to be responsible for this problem.

AlN has a strong affinity for oxygen; this results in the formation of solid solution Al(N, O) and polytypes. The thermal conductivity of aluminium nitride single crystal is a strong function of dissolved oxygen and decreases with increasing dissolved oxygen content [1]. In these conditions, sintered additives (mainly Y_2O_3) used to facilitate sintering, i.e. to ensure cohesion between grains, should not introduce additional oxygen into the AlN matrix or, even better, can be used to reduce the oxygen content of the AlN starting powder.

Defects present in the sintered materials can be divided into two groups. The first group comprises defects located at the boundaries between adjoining AlN crystal grains of a polycrystalline sample. They are mainly second phases, resulting from sintering additives, whose topology and nature are of importance in maintaining the thermal properties of the AlN ceramic. The second group consists of defects in the crystal lattice itself which can also affect the phonon scattering: i.e. thermal conductivity.

This paper deals with the second group of defects and is devoted to the characterization of dislocations and extended defects found in the AlN grains.

2. The würtzite structure

The würtzite structure can be described in terms of closed packed planes whose stacking along the c-axis can be written as Aa, Bb, Aa, Bb where, for example, A, B denote planes of N atoms and a, b planes of Al atoms. This notation is similar to that used for cubic semi-conductors with zincblende structure [3]. The shortest unit translation which is expected to be the Burgers vector of perfect dislocations is of $a/3\langle 11\bar{2}0\rangle$ type. These dislocations can dissociate in the basal plane following the reaction

$$a/3\langle 11\bar{2}0\rangle \rightarrow a/3\langle 10\bar{1}0\rangle + a/3\langle 01\bar{1}0\rangle \quad (1)$$

faulting the lattice so that a zincblende slice is formed

Aa, Bb, Cc, Aa, Cc, Aa, Cc

provided that the shear takes place between b, A plane, i.e. in the glide set between close atomic planes. Such a dissociation has already been shown in II–VI compounds like CdS, CdSe, ZnO (see, for example, [4]) and also in thin platelets of AlN grown from the vapour phase [5, 6]. The primary glide plane of the würtzite structure has been found to be the basal plane which is consistent with the previous dissociation reaction but other glide systems have been conjectured [7].

3. Experimental procedure

Sintered AlN samples with different addition of Y_2O_3, as a sintering additive, were obtained from Ceramiques Techniques Desmarquest (Trappes, France) [8]. Concentrations of Y_2O_3 ranged from 1% to 20% of the total initial powders. Samples used in this study are referenced to in the paper as Na 3.19 (1% Y_2O_3), Na 12.3 (0.5% CaF_2 + 2.5% Y_2O_3), Na 16.1 (20% Y_2O_3). The sintering temperature was usually 1 h at 1700° C. Discs 3 mm in diameter were cut from these samples and then mechanically polished down to 80 μm. They were then ion thinned to obtain electron beam transparency. Thin foils were observed in a Jeol 200 CX electron microscope operating at 200 kV.

4. Results

4.1. Dislocation observations

Dislocations in AlN grains appear mainly as sub-

0022–2461/89 $03.00 + .12

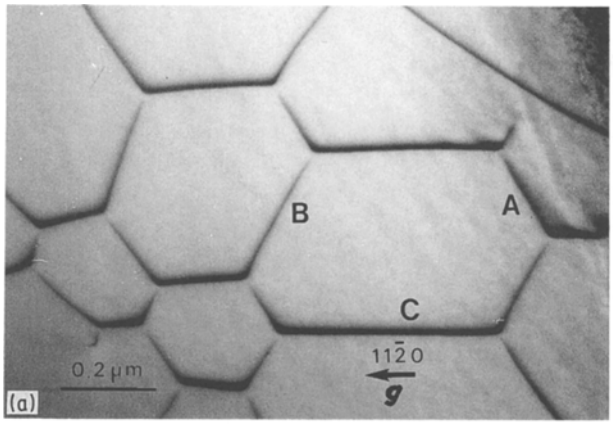

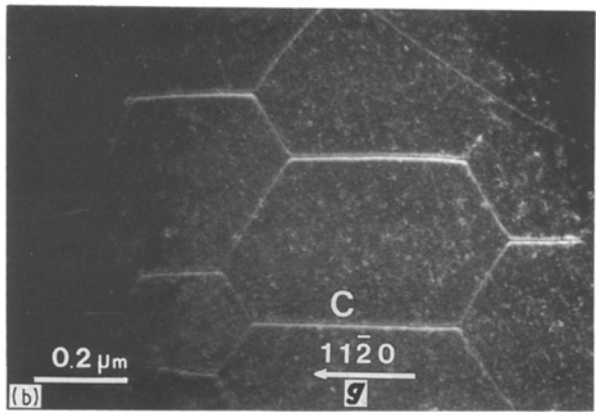

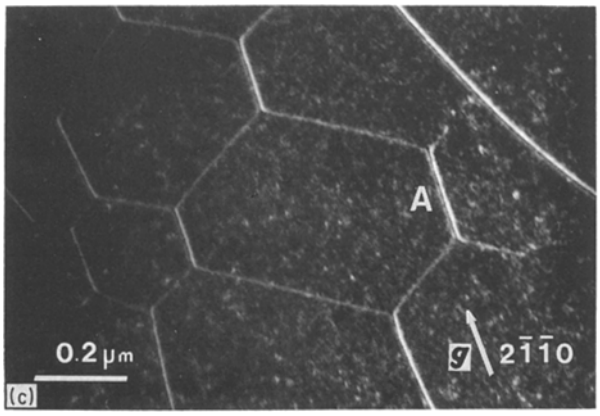

Figure 1 Na 12.3. Dislocations network in AlN formed by the glide of three sets of dislocations A, B, C. (a) Bright field ($\boldsymbol{g} = 11\bar{2}0$). (b) Weak-beam dark field, the dissociation of dislocation C is shown ($\boldsymbol{g} = 11\bar{2}0$, $3\boldsymbol{g}$ excited). (c) Weak-beam dark field, the dissociation of dissociation A is shown ($\boldsymbol{g} = 2\bar{1}\bar{1}0$), $3\boldsymbol{g}$ excited).

boundaries and pile-ups. It suggests that during the sintering process, AlN grains are plastically deformed. Usually dislocation configurations are found to result from glide and climb which is required to build up sub-boundaries. This is in agreement with the high-temperature treatment during sintering. Most of the dislocations have a Burgers vector of the $a/3\ \langle 11\bar{2}0\rangle$ type. Some hexagonal networks have also been found to be stabilized in the usual glide plane of the würtzite structure, i.e. the (0001) basal plane. That is the case for the dislocations configuration shown in Fig. 1. Contrast experiments show that this hexagonal network is built with three sets of dislocations, A, B, C, whose characteristics are listed in Table I.

These dislocations appear to be screw dislocations. Nodes as well as straight dislocation segments are dissociated, partial dislocations being of $a/3\ \langle 1100\rangle$ type which is consistent with Reaction 1. These dissociations can only be shown using the weak beam technique. The dissociation widths are the same on the three sets of the straight screw dislocations. The splitting width is found to be 8 ± 1 nm which is far lower than that found previously [5, 6]. Note that in the latter studies dissociations were imaged using dynamical conditions.

TABLE I

Dislocations	b	l	Dissociation
A	1/3 [2$\bar{1}\bar{1}$0]	2$\bar{1}\bar{1}$0	1/3 [10$\bar{1}$0] + 1/3 [1$\bar{1}$00]
B	1/3 [1$\bar{2}$10]	1$\bar{2}$10	1/3 [1$\bar{1}$00] + 1/3 [0$\bar{1}$10]
C	1/3 [11$\bar{2}$0]	11$\bar{2}$0	1/3 [10$\bar{1}$0] + 1/3 [01$\bar{1}$0]

4.2. Planar defects

Planar defects are found in all the samples whatever the concentration of Y_2O_3 in the starting powder. These defects emanate from and terminate in grain boundaries or second phases. In some cases, though, these defects can completely enclose a part of crystal in a grain (Fig. 2). These defects show fringe contrast similar to stacking faults, but unlike stacking faults they generally zigzag around and seem not to be confined to a particular crystallographic plane. However, in some cases, section of defects lying in a crystallographic plane can be observed which abruptly switch to another plane.

Geometry and characteristics of these defects have been determined using various diffraction conditions. Examples of these different geometries of defects are given below.

The defect shown in Fig. 3 is representative of the usual geometry of extended defect found in AlN whatever the additive concentration is. Rather than a stacking fault it looks like an antiphase boundary zigzagging between two domains where the atomic order is different.

The defect of Fig. 4 is an example of a stepped defect. It lies on different crystallographic planes which have been found to be (0001) for the G part and (1$\bar{1}$00) for the F part. A dislocation (C) is found

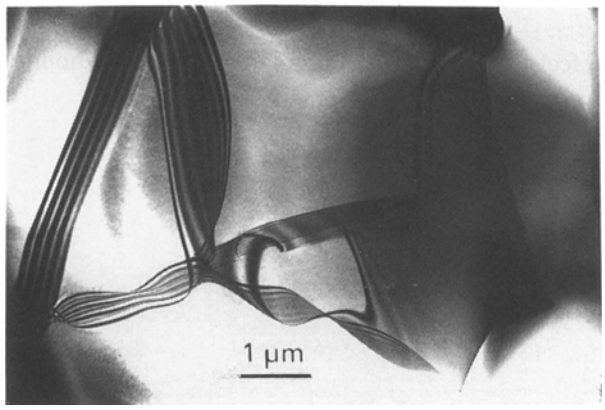

Figure 2 Na 3.19. AlN grain with second phases at grain boundaries. Planar defects are emanating from the grain boundaries.

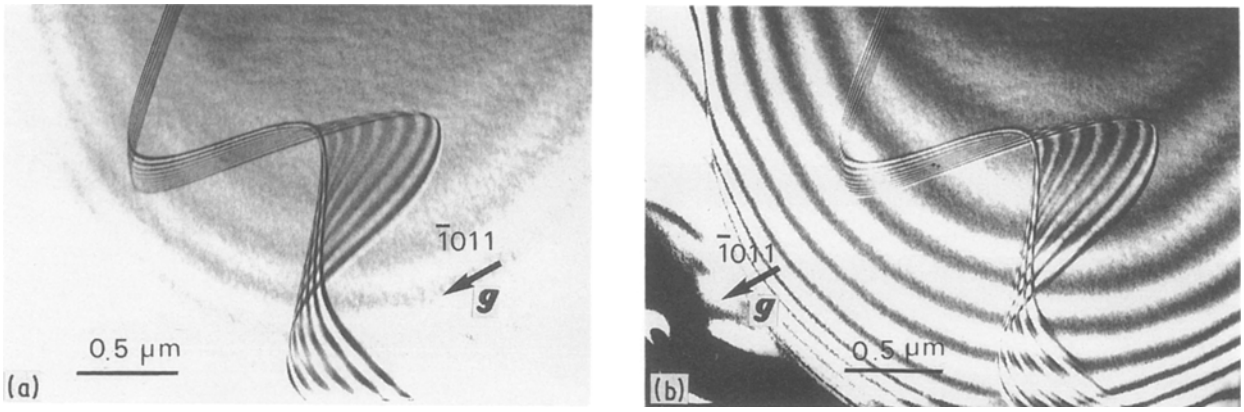

Figure 3 Na 12.3. Details of an antiphase boundary-like defect ($\boldsymbol{g} = \bar{1}011$). (a) Bright field. (b) Dark field.

at the intersection of these two planar sections along the $[1\,1\,\bar{2}\,0]$ direction.

Another kind of defect is found in the samples heavily charged in Y_2O_3 (20%). Contradictorily to what was found in the other materials, this defect evolves under the action of the electron beam. Dislocation loops are created in the immediate vicinity of the planar defect during observation (Fig. 5). The planar defect itself is not affected and lies in the $(1\,\bar{2}\,1\,0)$ plane. The dislocation loops have been found to be perfect loops of Burgers vector $a/[1\,\bar{2}\,1\,0]$ lying on the $(1\,\bar{2}\,1\,0)$ plane. They are perfect edge loops of the vacancy type, so they result from the aggregation of vacancies in stoichiometric ratio.

Although these three types of defect could be different in nature looking at their different geometric features, it appears that they behave the same way in diffraction experiments.

Numerous diffraction experiments were performed on these defects in order to characterize their displacement vector. They have been found to be out of contrast for $\boldsymbol{g} = 0\,1\,\bar{1}\,0,\ 1\,1\,\bar{2}\,0,\ 1\,\bar{2}\,1\,0$. When in contrast, fringes due to the planar defect are symmetrical in bright field and asymmetrical in dark field. No differences in orientation and contrast were found between the two halves of the crystal across the defect. This suggests that these defects are associated with a rigid body translation parallel to $[0\,0\,0\,1]$. However, these experiments failed to determine a simple ratio, n, for a translation vector $\boldsymbol{R} = c/n\,[0\,0\,0\,1]$ ($n \neq 1, 2, 3$).

5. Discussion

5.1. Stacking fault energy of AlN

To derive the value of the stacking fault energy from the dissociation width, elastic constants of AlN single crystals are needed. No single crystal values are reported in the literature and elastic modulus measured on ceramic materials seems to be very weak compared to that expected for single crystals. In these conditions we estimated the shear modulus from the theory [9] in which for semi-conductors μ can be expressed as

$$\mu = (32/9)(e^2/a^4)\,C^* \qquad (2)$$

where C^* is a reduced shear modulus which can be estimated from the ionicity factor, f_i, of the compound, e is the electron charge and a the lattice parameter. For AlN $f_i = 0.449$, so that C^* is estimated from theory to be equal to 0.35. This gives $\mu = 0.30 \times 10^{11}$ Pa. The stacking fault energy deduced from our measurements (using $\nu = 0.3$) is then 7.5 ± 0.9 mJ m^{-2} and the stacking fault energy reduced to one atom ($\gamma' = \sqrt{3}/4a^2\gamma$) is $\gamma' = 19 \pm 2.5$ meV at^{-1}.

Takeuchi *et al.* [4] looked for a correlation between reduced stacking fault and the nature of the chemical bond between atoms and found that reduced stacking fault energies (SFE) of III–V and II–VI compound semiconductors can be correlated to the charge redistribution index, s [10]. Using the s value of AlN ($s = -2.76$), the γ' value for AlN has been reported on the figure of Takeuchi *et al.* [4]. It is found that the relation between the reduced SFE and the charge

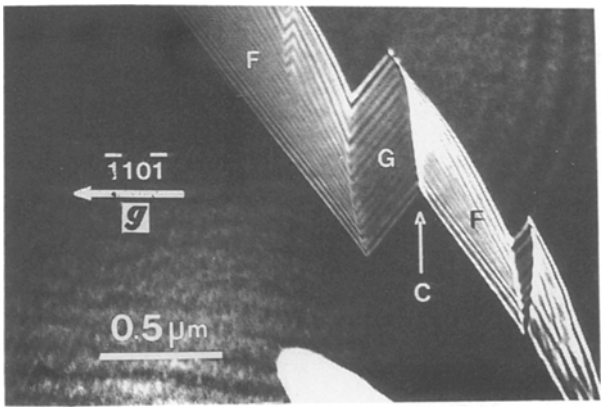

Figure 4 Na 12.3. Stepped defects. Weak-beam dark field ($\boldsymbol{g} = \bar{1}\,1\,0\,\bar{1}$, $2\boldsymbol{g}$ excited).

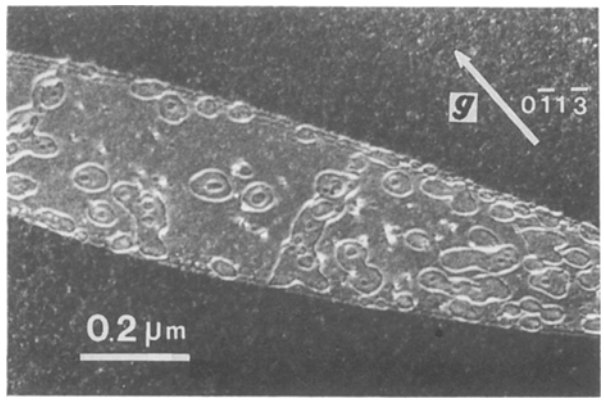

Figure 5 Na 16.1. Planar defects and nucleation of perfect vacancy loops during TEM observations (weak-beam dark field $\boldsymbol{g} = 0\,\bar{1}\,1\,\bar{3}$, $2\boldsymbol{g}$ excited).

redistribution index, s, still hold for AlN. This confirms the hypothesis of Takeuchi *et al.* that the s value plays a dominant role in the electrostatic energy contribution to the SFE which stabilizes the würtzite structure.

5.2. Planar defects

From the geometrical features and contrast characteristics of the planar defects reported above, one can retain several hypotheses for the formation of these defects. They are not relevant to the stacking faults found in between the partial dislocations in the dissociation of $a/3\langle 1\,1\,\bar{2}\,0\rangle$ dislocations. Such a dissociation process yields a stacking fault displacement vector of the type $a/3\langle 1\,\bar{1}\,0\,0\rangle$ which is not coherent with what was found in diffraction experiments. Furthermore this stacking fault is restricted to the basal plane and it has been shown that dislocation dissociation leads to small splitting widths. Neither of these planar defects are relevant to the analysis of Drum [11] who found stacking faults on $(0\,0\,0\,1)$ and $(\bar{1}\,2\,\bar{1}\,0)$ with displacement vectors of, respectively, $1/6\,[2\,0\,\bar{2}\,3]$ and $1/2\,[1\,0\,\bar{1}\,1]$ in AlN grown by vapour deposition.

Antiphase boundaries between impinging domains where the atomic order has been nucleated differently during the growing process could be an explanation for the formation of these defects. Such an ordering cannot be due to aluminium and nitrogen atoms only but to Al(N, O) solid solution where oxygen atoms found in some nitrogen sites have a local order. Such an explanation has to be ruled out because no extra spots corresponding to a substructure appear superimposed to the diffraction pattern of AlN. Furthermore, even if these spots do not appear as a consequence of the low scattering factor of oxygen for electrons, such antiphase boundaries would be in contrast using only substructure reflections. This is not the case.

Another hypothesis could be the formation of inversion domains (improperly called antiphase domains) [12, 13]. These usually result from the growth of A.B compound semi-conductors on a substrate which exhibits atomic steps on the surface. An inversion domain boundary (IDB) is then formed at the plane where two crystals with different polarity coalesce during the growth on a non-polar substrate. This results along this plane in A–A and B–B bonds, for example, in the place where a perfect crystal had A–B bonds. The phase change experienced by an electron beam when it crosses an IDB is the sum of the phase change, which is due to the change of the structure factor and a phase change of $2\pi \boldsymbol{g}\boldsymbol{R}$ due to relative displacement across the fault plane. The relative displacement $\boldsymbol{R}$ is caused by the different bond lengths between like atoms at the IDB. From our diffraction contrast experiments such defects cannot be ruled out if an $\boldsymbol{R}$ contrast is assumed. This has been found in GaAs [13]. However, these incorrect bondings are expected to be energetic in covalent crystals and are associated with very constraining boundary conditions which are not likely to occur during the sintering process.

More likely, these defects could be associated with the incorporation of oxygen in the lattice. Oxygen

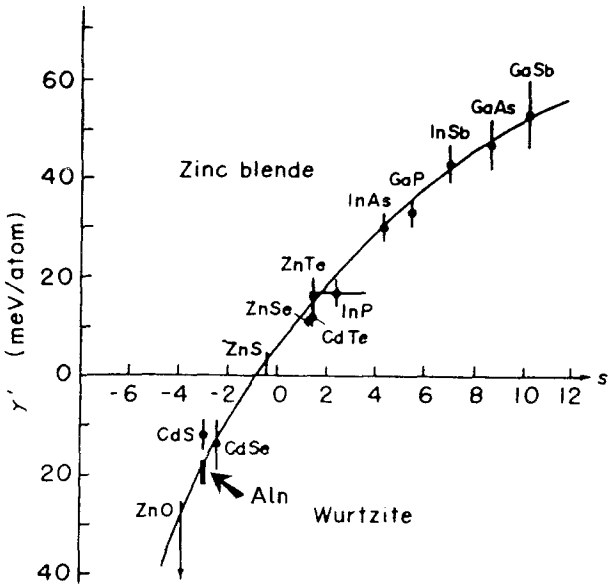

Figure 6 Relation between the reduced SFE and the charge redistribution index s (from [4]). The γ' value of AlN has been added to the original drawing.

incorporation in the AlN matrix can be formally expressed by the equation

$$Al_2O_3 + 3V_{Al} + 3V_N \rightarrow V_{Al} + 2Al_{Al} + 3O_N$$

This incorporation is accompanied by a volume change in the matrix [1] because the covalent radius of tetravalent oxygen is lower than that of nitrogen; furthermore, an aluminium vacancy is required for the balance equation. Then substituting oxygen at the planar defect sites yields a size effect relative to oxygen radius and a reorganization of aluminium atoms. A rigid body translation whose length is a fraction of a typical translation of the lattice plus a structure factor change is expected. The incorporation of oxygen at interface-like planar defects rather than as bulk solid solution Al(N, O), can be explained if the planar defects derive from an oxidation product which initially costs individual grains more uniformly. This is coherent with the observation of extended defects completely surrounding some regions inside AlN grains or the fact that they emanate from second phases at grain boundaries. These planar defects can move with local migration of oxygen atoms and aluminium vacancies. It seems plausible that they can also act as high diffusivity paths as is usually the case for extended defects. Formation of second phases at grain boundaries (which are double oxides of yttrium and aluminium [14]) requires addition of aluminium and oxygen to Y_2O_3 by diffusion out of the AlN matrix. This can be achieved through these planar defects which can also provide oxygen from the matrix into the second phases present at grain boundaries; this leads to compositional changes near the defects. From that point, the concentration of point defects in the immediate vicinity of planar defects can change as a function of the Y_2O_3 content of the starting powder. When locally the concentration of vacancies is in stoichiometric ratio in the two sublattices the electron beam can induce aggregation of point defects. This is illustrated in Fig. 5 where vacancy condensation

occurs under electron-beam irradiation for samples highly charged with Y_2O_3.

6. Conclusion

Extended defects in sintered AlN have been found to be dislocations and planar defects. Dissociated dislocations were shown using the weak beam technique. The splitting widths were found to be considerably lower than those measured previously [5, 6] and yield a stacking fault energy $\gamma = 7.5 \pm 1\,\mathrm{mJ\,m^{-2}}$ and a reduced stacking fault energy $\gamma' = 19 \pm 2.5\,\mathrm{meV\,at^{-1}}$, which shows the same correlation with the charge redistribution index as in the other II–VI compounds. Amongst the possible hypotheses for the formation of extended planar defects whose topology can be relevant to APB or IDB, contrast analysis and geometrical features have been explained to be associated with the incorporation of oxygen atoms in the AlN matrix during oxidation of a product which initially costs individual grains of AlN.

Acknowledgements

M. P. Braudeau (Ceramiques Techniques Desmarquest) is thanked for helpful discussions and for supplying the AlN samples. The authors also thank H. Garem (LMP Poitiers) for assistance during this study. This work was funded by an MRT contract number 85.S.0435.

References

1. G. A. SLACK, *J. Phys. Chem. Solids* **34** (1973) 321.
2. W. WERDECKER and F. ALDINGER, *IEEE Transactions on components, and manufacturing technology CHMT7* **4** (1984) 399.
3. J. P. HIRSH and J. LOTHE, "Theory of Dislocations" (Wiley, New York, 1982) p. 313.
4. S. TAKEUCHI, K. SUZUKI, K. MAEDA and H. IWANAGA, *Phil. Mag. A* **5** (1984) 171.
5. P. DELAVIGNETTE, H. B. KIRKPATRICK and S. AMELINCKX, *J. Appl. Phys.* **32** (1961) 1098.
6. H. BLANK, P. DELAVIGNETTE and S. AMELINCKX, *Phys. Status Solidi* **2** (1962) 1660.
7. YU. A. OSIPIYAN and I. S. SMIRNOVA, *ibid.* **30** (1968) 19.
8. PH. BRAUDEAU, B. CALES and J. P. TORRE, "Science of Ceramics", edited by D. Taylor (Butler and Tanner Ltd., London, 1987) Ch. 14, p. 413.
9. J. C. PHILLIPS, "Bonds and Bands in Semiconductors" (Academic, New York, London, 1973) p. 73.
10. J. C. PHILLIPS and J. A. VAN VECHREN, *Phys. Rev. Lett.* **23** (1969) 1115.
11. C. M. DRUM, *Phil. Mag.* **11** (1965) 313.
12. D. B. HOLT, *J. Phys. Chem. Solids* **30** (1969) 1297.
13. N. H. CHO, B. C. DE COOMAN, C. B. CARTER, R. FLETCHER and D. K. WAGNER, *Appl. Phys. Lett.* **47** (1985) 879.
14. M. F. DENANOT and J. RABIER, *Mater. Sci. and Engng A*, in press.

Received 7 April
and accepted 1 August 1988